The First Examples of Alkali Metal/Cu/Ce/Chalcogenides: The Layered Heterometallic Compounds $KCuCe_2S_6$ and $K_2Cu_2CeS_4$

Anthony C. Sutorik,[†] Joyce Albritton-Thomas,[‡] Carl R. Kannewurf,[‡] and Mercouri G. Kanatzidis*[,†,§]

Contribution from the Department of Chemistry and Center for Fundamental Materials Research, Michigan State University, East Lansing, Michigan 48824, and Department of Electrical Engineering and Computer Science, Northwestern University, Evanston, Illinois 60208

Received February 11, 1994[⊗]

Abstract: From the reaction of the metallic elements in molten alkali metal/polychalcogenide fluxes, we have synthesized $KCuCe_2S_6$ (I) and $K_2Cu_2CeS_4$ (II). Isolated from a 2/0.5/1/8 mixture of K_2S/Cu/Ce/S heated at 270 °C for 6 d, I crystallizes in the space group $C2/c$ (no. 15) with $a = 6.859(2)$ Å, $b = 21.154(2)$ Å, $c = 6.8599(8)$ Å, $\beta = 105.41(2)°$, and $Z = 4$. The structure of I features $(CuCe_2S_6)_n^{n-}$ anionic layers composed of $[CeS_8]$ bicapped trigonal prisms connected in the $ZrSe_3$ fashion with Cu^+ residing in tetrahedral sites within the layers and K^+ cations in the interlayer gallery. Diffuse reflectance measurements have shown an approximated band gap of 1.8 eV for I, and magnetic studies exhibit Curie–Weiss paramagnetic behavior at temperatures above 160 K with $\mu_{eff} = 3.08\ \mu_B$/formula. Isolated from a 4.2/0.5/0.25/8 mixture of the above reagents heated at 260 °C for 5d, II crystallizes in the $C2/m$ space group (no. 12) with $a = 14.320(3)$ Å, $b = 3.961(1)$ Å, $c = 7.496(2)$ Å, $\beta = 109.77(2)°$, and $Z = 2$. Compound II is also a layered structure in which Ce atoms, octahedrally coordinated by S, and Cu, tetrahedrally coordinated by S, form anionic layers related to Mg_2SiO_4 (olivine) with K^+ in the interlayer gallery. From magnetic susceptibility studies, a μ_{eff} of 2.38 μ_B was estimated above 150 K corresponding to the value for a lone Ce^{3+}. The compound's oxidation states are formalized as $K_2(Cu^{1+})_2(Ce^{3+})(S^{2-})_3(S^{1-})$. Below 150 K, the material shows non-Curie–Weiss behavior, exhibiting a decreasing μ_{eff}. Thermopower studies on II show p-type carriers; however, the conductivity is low and increases with increasing temperature, suggesting a low carrier mobility possibly arising from small polaron formation.

Introduction

One of the key features of the high-Tc copper oxide superconductors is the high degree of covalency present in the Cu–O bonds which has been found to be directly correlated to increasing critical temperatures.[1] This covalency arises through the high concentration of electropositive cations present in these structures which favor the stabilization of higher oxidation states for copper. Compounds containing heterometallic mixtures of either two different alkaline-earth metals (as in $Tl_2Ba_2Ca_2Cu_3O_{10}$)[2] or an alkaline-earth and lanthanide (as in $La_{2-x}(Ca,Sr,Ba)_xCuO_4$)[3] seem to stabilize the appropriate mixed-valency and high oxidation state that is necessary (but of course not sufficient) for superconductivity. In order to achieve mixed-valency and higher oxidation states, the search for new materials in other quaternary systems containing mixtures of strongly electropositive cations becomes intriguing. Such investigations would be useful in further elucidating the role electropositive cations play in the stability of certain transition metal oxidation states and may lead to the discovery of materials with novel structures and properties.

Our group and others have demonstrated the utility of reacting transition metals in molten alkali metal/polychalcogenide (A_2Q_x) fluxes as a synthetic route to new ternary compounds.[4,5] Many of these compounds are obtained due to the low reaction temperatures used (as compared to those for typical solid-state techniques). The A_2Q_x fluxes have melting points ranging from 250 to 450 °C, depending on the alkali metal/polychalcogenide combination, and once molten, the flux acts as both reagent and medium in the subsequent reaction with the transition metal.

Our approach has been to simply react a lanthanide and transition metal in a molten A_2Q_x flux at the same time. We have begun our investigations using A/Cu/Ce/Q systems because separately both metals have shown reactivity in molten polychalcogenide salts, which has led to the isolation of new compounds.[4,6,7] Although some studies have been made into Cu/Ce/Q systems,[8] prior to our work, no quaternary examples, with alkali metals as the fourth element, had been characterized. We now report our first two lanthanide/transition metal quaternary compounds: $KCuCe_2S_6$ and $K_2Cu_2CeS_4$. The former compound possesses Cu^+ vacancies created by the distribution of Cu^+ atoms over a large excess of tetrahedral sites, which could give rise to

† Michigan State University.
‡ Northwestern University.
§ Camille and Henry Dreyfus Teacher Scholar, 1993–95.
⊗ Abstract published in *Advance ACS Abstracts,* July 1, 1994.

(1) Sleight, A. W. *Chemistry of High-Temperature Superconductors;* ACS Symposium Series 351; American Chemical Society: Washington, DC, 1987; Chapter 1, p 2.

(2) (a) Sheng, Z. Z.; Herman, A. M. *Nature* **1988**, *332*, 138–139. (b) Parkin, S. S.; et al. *Phys. Rev. Lett.* **1988**, *61*, 750–753.

(3) (a) Bendorz, J. G.; Muller, K. A. *Z. Phys.* **1986**, *B64*, 189–193. (b) Cava, R. J.; vanDover, R. B.; Batlogg, B.; Reitman, E. A. *Phys. Rev. Lett.* **1987**, *58*, 408–410.

(4) (a) Kanatzidis, M. G. *Chem. Mater.* **1990**, *2*, 353–363. (b) Kanatzidis, M. G.; Park, Y. *J. Am. Chem. Soc.* **1989**, *111*, 3767–3769. (c) Kanatzidis, M. G.; Park, Y. *Chem. Mater.* **1990**, *2*, 99–101. (d) Park, Y.; Kanatzidis, M. G. *Angew. Chem., Int. Ed. Engl.* **1990**, *29*, 914–915.

(5) (a) Sunshine, S. A.; Kang, D.; Ibers, J. A. *J. Am. Chem. Soc.* **1987**, *109*, 6202–6204. (b) Kang, D.; Ibers, J. A. *Inorg. Chem.* **1988**, *27*, 549–551.

(6) Sutorik, A. C.; Kanatzidis, M. G. *Angew. Chem., Int. Ed. Engl.* **1992**, *31*, 1594–1596.

(7) (a) McCarthy, T.; Zhang, X.; Kanatzidis, M. G. *Inorg. Chem.* **1993**, *32*, 2944–2948. (b) Park, Y.; Kanatzidis, M. G. *Chem. Mater.* **1991**, *3*, 781–783. (c) Park, Y.; Degroot, D.; Schindler, J.; Kannewurf, C. R.; Kanatzidis, M. G. *Angew. Chem., Int. Ed. Engl.* **1991**, *30*, 1325–1328.

(8) Observed phases have been $CuCeQ_2$ (Q = S, Se), having $CuLaS_2$ structure type,[8a] Ce_5CuSe_8, which has the Th_3P_4 structure type,[8b] and two phases of uncharacterized structure, $Ce_4Cu_2S_7$[8c] and Ce_2CuTe_4.[8d] (a) Julien-Pouzol, M.; Guittard, M. *Ann. Chim. (Paris)* **1972**, *7*, 253–262. (b) Julien-Pouzol, M.; Guittard, M. *Bull. Soc. Chim. Fr.* **1968**, *6*, 2293–2295. (c) Collin, G.; Rouyer, F.; Loriers, J. *C. R. Seances Acad. Sci., Ser. C* **1968**, *266C*, 689–691. (d) Pardo, M.-P.; Dung, N. H. *C. R. Seances Acad. Sci., Ser. 2* **1987**, *304* (12), 637–639.

0002-7863/94/1516-7706$04.50/0

ionic conductivity. The latter compound exhibits valence fluctuations that result in enhanced electrical polaron-like conductivity. This paper details their synthesis, structure, and physical properties.

Experimental Section

Reagents. The following reagents were used as obtained: cerium, 40 mesh, Johnson M. Matthey Co., Ward Hill, MA; copper metal, Fisher Scientific Co., Fairlawn, NJ; sulfur powder, sublimed, JT Baker Co., Phillipsburg, NJ; potassium metal, analytical reagent, Mallinckrodt Inc., Paris, KY. The dimethylformamide (DMF) used was obtained in analytical reagent grade from EM Science, Inc., Gibbstown, NJ.

Potassium Sulfide, K_2S. The following procedure was modified from that given in the literature.[9] A 7.094-g (182 mmol) sample of K was sliced in an N_2-filled glovebox and combined with 2.908 g (91 mmol) of S into a 250-mL round-bottom flask. The flask was chilled to −78 °C using a dry ice/acetone bath, and approximately 100 mL of NH_3 was condensed, under an N_2 atmosphere, onto the reagents, giving a dark blue solution. The solution was stirred via a magnetic stir bar while the liquid NH_3 was allowed to slowly evaporate off (approximately 8 h) under a flow of N_2. A second portion of NH_3 was usually added and the evaporation repeated to insure complete reaction of the reagents. The resulting yellow product was evacuated on a Schlenk line overnight and then taken into an N_2-filled glovebox where it was ground to a fine powder and stored.

Potassium Copper(I) Dicerium(III) Hexasulfide, $KCuCe_2S_6$ (I). A 0.110-g (1.0 mmol) sample of K_2S, 0.016 g (0.25 mmol) of Cu, 0.070 g (0.50 mmol) of Ce, and 0.128 g (4.0 mmol) of S were weighed into a vial in an N_2-filled glovebox. The starting materials were mixed thoroughly and loaded into a Pyrex tube. The tube was then evacuated to $<3 \times 10^{-3}$ mbar and flame-sealed. The reaction was heated to 270 °C over 12 h, held at that temperature for 6 days, and cooled to 120 °C at 3 °C/h, followed by quenching to 50 °C. The product was isolated by dissolving away residual K_2S_x flux with a successive washing of degassed DMF under N_2 flow, in order to prevent oxidation of polysulfide to sulfur. Polysulfides dissolved in DMF give a dark blue-green solution when concentrated, and the isolation was continued by carefully decanting the concentrated DMF and replacing it with a fresh portion until such an addition remained clear, signaling complete K_2S_x removal. The remaining material was red microcrystalline needles of I; a yield of 68%, based on Ce, is typical. The purity of the material was confirmed by comparing the product's X-ray powder diffraction pattern with one calculated using data from the single crystal study. The product was insoluble in water, methanol, and DMF and is stable in air for extended periods.

The above reaction was found to yield good quality product over a temperature range from 260 to 350 °C. At temperatures greater than 350 °C, a yellow powder of CeS_2 begins to contaminate I. Typically, I is microcrystalline, but single crystals were obtained by doubling the amounts of K_2S and S, hence doubling the amount of flux, and running the reaction at 350 °C for 5 days, cooling at 2 °C/h. However, this procedure also results in a small amount of CeS_2 powder mixed with the single crystals of I.

Dipotassium Dicopper(I) Cerium(III) Tetrasulfide, $K_2Cu_2CeS_4$ (II). A single phase of II was obtained by the reaction of 0.231 g (2.09 mmol) of K_2S, 0.016 g (0.25 mmol) of Cu, 0.018 g (0.125 mmol) of Ce, and 0.128 g (4.0 mmol) of S. The reagents were loaded into Pyrex tubes and evacuated in the manner described for I. The reaction was heated to 260 °C over 12 h, held at that temperature for 5 days, and cooled to 210 °C at 2 °C/h, followed by quenching to room temperature. The product was isolated using one portion of degassed distilled water (left in contact with the sample for only 10–20 min) and several portions of degassed DMF in a manner similar to that described for I. The remaining material was black microneedles of II. The purity was checked by comparing the X-ray powder diffraction pattern of the product to one calculated from single crystal X-ray data, and typically, a small amount of CeO_2 (1–5%) was seen as an impurity. Taking this into account, an approximate yield of 70%, based on Cu, was estimated for II. The product was insoluble in methanol and DMF and appears stable in dry air for extended periods. Although stable in distilled water for a short time (<12 h), prolonged exposure causes decomposition to CeO_2 and presumably soluble Cu-containing species.

As with I, the purity of II is very dependent on reaction temperature. Here, any temperature above 260 °C will result in impurities of KCu_4S_3 and some as a yet unknown phase. Black, brick-shaped single crystals of II, suitable for X-ray diffraction studies, were obtained by increasing the amount of K_2S to 0.248 g (2.25 mmol) and increasing the reaction temperature to 420 °C for 5 days (cooling at 2 °C/h) but were accompanied by the above-mentioned impurities.

Physical Measurements. Powder X-ray Diffraction. Analyses were performed using a calibrated Rigaku Rotaflex rotating anode powder diffractometer controlled by an IBM computer and operating at 45 kV/100 mA, employing Ni-filtered Cu radiation.

Infrared Spectroscopy. Infrared spectra, in the far-IR region (600–50 cm^{-1}), were recorded with a computer-controlled Nicolet-740 Fourier transform infrared spectrophotometer in 4-cm^{-1} resolution. Analyses were performed on solid samples using CsI as the pressed pellet matrix.

UV/Vis/Near-IR Spectroscopy. Optical diffuse reflectance measurements were performed at room temperature using a Shimadzu UV-3101PC double-beam, double-monochromator spectrophotometer. The instrument is equipped with an integrating sphere and controlled by AN AST BRAVO 3/25S personal computer. The reflectance versus wavelength data generated can be used to estimate a material's band gap by converting reflectance to absorption data using the Kubelka–Munk function as described elsewhere.[10]

Magnetic Susceptibility. The magnetic response of the compounds was measured over the range 2–300 K using a MPMS Quantum Design SQUID magnetometer. Samples were ground to a fine powder to minimize possible anisotropic effects, and corrections for the diamagnetism of the PVC sample containers were applied. Magnetic susceptibility as a function of field strength (at a constant temperature of 300 K) was first investigated to determine if the samples experienced saturation of their magnetic signal. For both compounds, magnetization increased linearly with increasing field over the range investigated (100–50 000 G). The subsequent temperature-dependent studies were performed at low to moderate field strengths (1000–2000 G).

Charge-Transport Measurements. Dc electrical conductivity studies were performed on both single crystals (approximately 0.5 mm in length) and pressed pellets, but thermopower measurements were made only on pressed pellets. Conductivity measurements were performed in the usual four-probe geometry with 60- and 25-μm-diameter gold wires used for the current and voltage electrodes, respectively. Measurements of the sample cross-sectional area and voltage probe separation were made with a calibrated binocular microscope. Conductivity data were obtained with the computer-automated system described elsewhere.[11] Thermoelectric power measurements were made by using a slow ac technique[12] which requires the production of a slowly varying periodic temperature gradient across the samples and measuring the resulting sample voltage. Samples were suspended between quartz block heaters by 60-μm gold wires thermally grounded to the block with GE 7031 varnish. The gold wires were used to support and conduct heat to the sample, as well as to measure the voltage across the sample resulting from the applied temperature gradient. The magnitude of the applied temperature gradient was generally 1.0 K. Smaller temperature gradients gave essentially the same results but with somewhat lower sensitivity. In both measurements, the gold electrodes were held in place on the sample with conductive gold paste. Mounted samples were placed under vacuum (10^{-3} Torr) and heated to 320 K for 2–4 h to cure the gold contacts. For a variable-temperature run, data (conductivity or thermopower) were acquired during sample warming. The average temperature drift rate during an experiment was kept below 0.3 K/min. Multiple variable-temperature runs were carried out for each sample to ensure reproducibility and stability. At a given temperature, reproducibility was within ±5%.

Single Crystal X-ray Diffraction. Intensity data for I and II were collected using a Rigaku AFC6S four-circle automated diffractometer equipped with a graphite crystal monochromator. An ω–2θ scan mode was used. The crystals' stability was monitored with three standard reflections whose intensities were checked every 150 reflections. No crystal decay was detected in either case. An empirical absorption correction based on ψ scans was applied to all data during initial stages of refinement. An empirical DIFABS correction[13] was applied after full isotropic

(9) Feher, F. *Handbuch der Praparativen Anorganischen Chemie*; Brauer, G., Ed.; Fedinand Enke: Stuttgart, Germany, 1954; pp 280–281.

(10) McCarthy, T. J.; Ngeyi, S.-P.; Liao, J.-H.; DeGroot, D. C.; Hogan, T.; Kannewurf, C. R.; Kanatzidis, M. G. *Chem. Mater.* **1993**, *5*, 331–340.

(11) Lyding, J. W.; Marcy, H. O.; Marks, T. J.; Kannewurf, C. R. *IEEE Trans. Instrum. Meas.* **1988**, *37*, 76–80.

(12) Marcy, H. O.; Marks, T. J.; Kannewurf, C. R. *IEEE Trans. Instrum. Meas.* **1990**, *39*, 756–760.

(13) Walker, N.; Stuart, D. *Acta Crystallogr.* **1983**, *A39*, 158–166.

Table 1. Crystallographic Data for $KCuCe_2S_6$ and $K_2Cu_2CeS_4$

	$KCuCe_2S_6$	$K_2Cu_2CeS_4$
a, Å	6.859(2)	14.320(3)
b, Å	21.154(2)	3.961(1)
c, Å	6.8599(8)	7.496(2)
β, deg	105.41(2)	109.77(2)
V, Å^3	959.6(6)	400.1(2)
space group	$C2/c$ (no. 15)	$C2/m$ (no. 12)
Z	4	2
fw, g/mol	575.24	473.65
d_{calcd}, g/cm^3	3.982	3.931
μ, cm^{-1}	133.09	129.27
cryst dimens, mm^3	0.02 × 0.04 × 0.5	0.04 × 0.08 × 0.2
radiation	Mo Kα	Mo Kα
$2\theta_{max}$	60.0°	60.0°
data coll. temp, °C	23	−80
no. of data collected	1552	505
total no. of unique data	1409	486
no. of data $F_o^2 > 3\sigma F_o^2$	1036	436
no. of variables	55	29
R/R_w,[a] %	3.2/5.7	2.0/2.6

[a] $R = \sum(|F_o| - |F_c|)/\sum|F_o|$. $R_w = \{\sum w(|F_o| - |F_c|)^2/\sum w|F_o|^2\}^{1/2}$.

Table 2. Selected Bond Distances (Å) and Angles (deg) for $KCuCe_2S_6$[a]

Ce(1)–S(1)	2.899(3) (×2)	Ce(2)–S(1)	2.880(3) (×2)
Ce(1)–S(2)	3.017(3) (×2)	Ce(2)–S(2)	2.992(3) (×2)
Ce(1)–S(3)^{a,f}	2.866(3)	Ce(2)–S(3)^{b,g}	2.885(3)
Ce(1)–S(3)^{c,d}	2.910(3)	Ce(2)–S(3)^{d,e}	2.885(3)
Cu(1)–S(2)	2.363(3) (×2)	Cu(2)–S(1)	2.18(1) (×2)
Cu(1)–S(3)^{a,b}	2.335(3)	Cu(2)–S(3)^{f,g}	2.451(9)
S(1)–S(2)	2.101(4)		
S(1)–Ce(1)–S(2)	41.55(8)	S(1)–Ce(2)–S(2)	41.88(8)
S(1)–Ce(1)–S(3)^{d}	83.68(8)	S(1)–Ce(2)–S(3)^{d}	84.46(8)
S(1)–Ce(1)–S(2)^{a}	88.73(8)	S(1)–Ce(2)–S(2)^{b}	90.86(9)
S(1)–Ce(1)–S(3)^{f}	81.38(8)	S(1)–Ce(2)–S(3)^{g}	81.75(8)
S(3)^{c}–Ce(1)–S(3)^{d}	93.9(1)	S(3)d–Ce(2)–S(3)^{c}	89.5(1)
S(2)–Cu(1)–S(2)^{b}	91.0(2)	S(1)–Cu(2)–S(1)^{a}	100.5(7)
S(2)–Cu(1)–S(3)^{b}	110.5(1)	S(1)–Cu(2)–S(3)^{g}	108.3(1)
S(2)–Cu(1)–S(3)^{a}	110.0(1)	S(1)–Cu(2)–S(3)^{f}	108.9(1)
S(3)^{a}–Cu(1)–S(3)^{b}	120.8(2)	S(3)f–Cu(2)–S(3)^{g}	120.3(7)

[a] Superscripts indicate symmetry equivalent atoms.

refinement, after which full anisotropic refinement was performed. The structure was solved by direct methods using SHELXS-86 software,[14a] and full matrix least squares refinement was performed using the TEXSAN software package.[14b] There were no significant residual electron density peaks in the final Fourier difference electron density map. The highest peak from either compounds was less than 1.3 e/A^3. Crystallographic data for **I** and **II** are given in Table 1. For atomic coordinates and anisotropic thermal parameters see the supplementary material.

Results and Discussion

$KCuCe_2S_6$ (I). Structure. Compound **I** forms a two-dimensional structure in which Cu, Ce, and S compose anionic layers and K resides in the interlayer gallery. There are two crystallographically distinct Ce sites; however, both have the same coordination environment. The Ce are coordinated by a bicapped trigonal prism of S atoms made of two $(S_2)^{2-}$ units forming the short sides of the prism and four S^{2-} ions at the apex and capping positions (Figure 1). The trigonal prisms stack in one dimension by sharing triangular faces (see Figure 2), forming chains parallel to [101]. Layers are formed when neighboring chains share monosulfides; this is done such that the monosulfides of the trigonal prisms in one chain are the capping monosulfides of the neighboring chains. This results in the $(Ce_2S_6)^{2-}$ portion of the structure being analogous to the known phase, $ZrSe_3$; however, $ZrSe_3$ exhibits elongated Zr–Se bonds between the chains (Zr–Se = 2.72–2.74 Å within the chain, Zr–Se = 2.87 Å between the chains).[15] The larger coordination sphere of the Ce easily accommodates the eight sulfur atoms, and in fact, the capping bonds are no longer than any of the other Ce–S bonds present (Table 2). A view of the Ce–S only portion of the anionic layers is shown in Figure 3a.

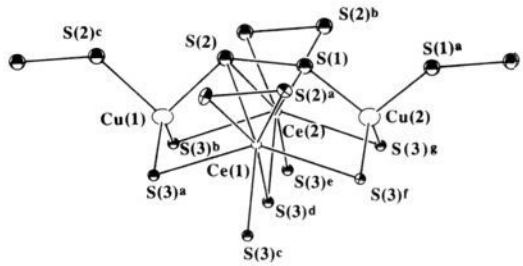

Figure 1. ORTEP representation of a fragment of the anionic layer of $KCuCe_2S_6$ showing the immediate coordination environment of the Ce^{3+} and Cu^+ cations. The large open ellipses represent Cu, the small open ellipses, Ce, and the ellipses with octant shading, S. Selected bond distances and angles are given in Table 2.

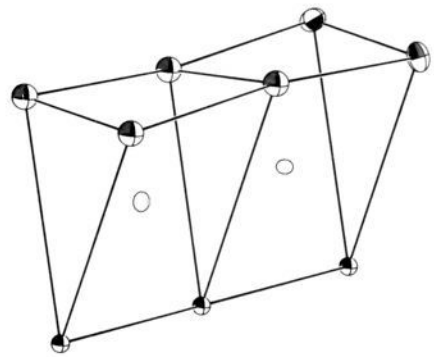

Figure 2. Face-sharing arrangement of the Ce-centered trigonal prisms in $KCuCe_2S_6$. The Ce are represented by the open ellipses, and S, by the ellipses with octant shading.

The Ce–S distances for **I** range from 2.838(1) to 3.010(1) Å and are comparable with those in previously reported compounds (2.878 Å in $KCeS_2$,[21g] 2.88–3.26 Å in CeS_2[16]). The disulfide bond of 2.105(3) Å is also reasonable.

The spaces between the Ce-centered prismatic chains are large enough that the compound's Cu^+ ions can be coordinated at tetrahedral sites within these intralayer grooves. Two crystallographically distinct Cu sites exist. Each is bonded at two points to the ends of two separate $(S_2)^{2-}$ units and at the remaining sites to monosulfides. The immediate coordination environment of the two Cu sites is also shown in Figure 1, and a full view of the extended structure, as seen parallel to the intralayer grooves (parallel to [101]), is shown in Figure 3b. Although two Cu sites are present, refinement of the multiplicity of those sites showed that a lone Cu atom is disordered over both sites. Each site resides on a mirror plane, giving then, crystallographically, $^1/_2$ occupancies, but when allowed to refine, the Cu(1) site occupancy becomes 0.427, where that for Cu(2) becomes 0.073. No disorder was found on the K^+ site. Bond distances are consistent on the more fully occupied Cu(1) site (2.363 and 2.335 Å) but exhibit a larger range on the Cu(2) site (2.18 and 2.45 Å), probably owing to the Cu(2)'s higher temperature factor, reflecting greater uncertainty in its position. The Cu sites alternate down the intralayer groove, and so would seem to indicate that Cu^+ conductivity through the grooves may be possible. This may lead to intriguing ion-exchange possibilities.

(14) (a) Sheldrick, G. M. In *Crystallographic Computing 3*; Sheldrick, G. M., Kruger, C., Doddard, R., Eds.; Oxford University Press: Oxford, England, 1985; pp 175–189. (b) Gilmore G. J. *Appl. Crystallogr.* **1984**, *17*, 42–46.

(15) Kroniert, W.; Plieth, K. *Z. Anorg. Allg. Chem.* **1965**, *336*, 207–218.

(16) (a) Marsh, R. E.; Herbstein, F. H. *Acta Crystallogr.* **1983**, *39B*, 280–287. (b) Yanagisawa, Y.; Kanamaru, F.; Kume, S. *Acta Crystallogr.* **1979**, *35B*, 137–139.

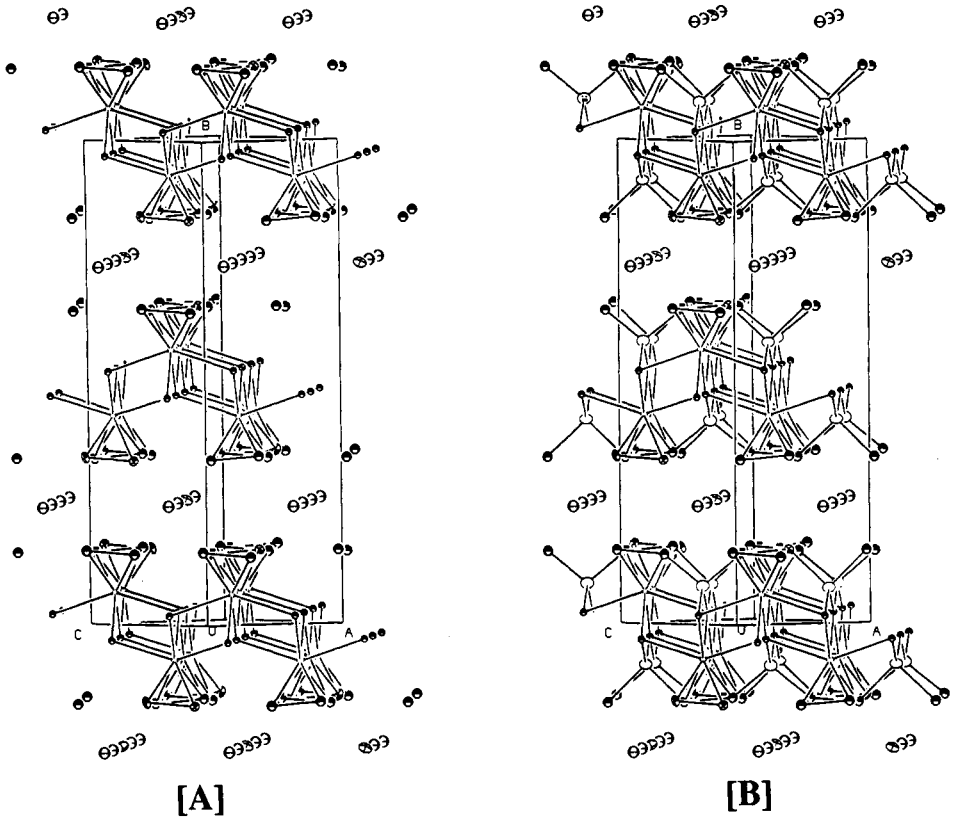

Figure 3. Two views of the extended structure of $KCuCe_2S_6$. The anionic layers, as seen down the [101] direction, are shown both (A) without and (B) with the compound's Cu atoms in the intralayer grooves. Ce is represented by small open circles, Cu, by large open circles, K, by nonshaded octant ellipses, and S, by shaded octant ellipses.

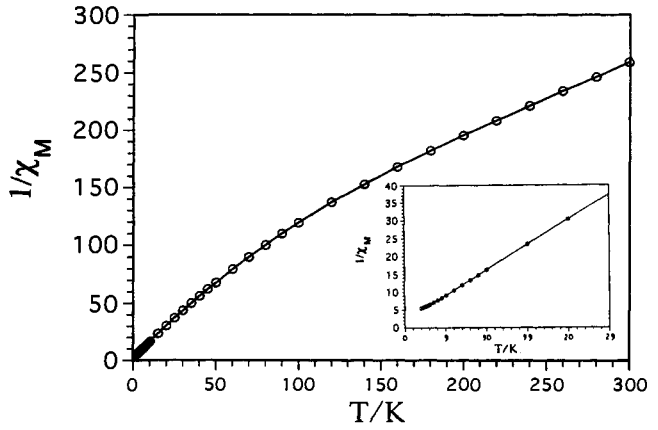

Figure 4. Plot of $1/\chi_M$ vs T for $KCuCe_2S_6$ taken at 2000 G over 2–300 K showing Curie–Weiss behavior above 160 K and negative deviations below 160 K. The inset graph shows an expanded view of the region 2–25 K.

There is also a correlation between Cu occupancy and the bonds between Ce and the disulfide. The more fully occupied Cu(1) is bonded to the S(2) atom of the disulfide which then has a Ce–S distance of 3.017(3) Å. Meanwhile, the S(1) atom coordinated to the lesser occupied Cu(2) site experiences shortened Ce–S bonds (2.880(2) Å). The lack of coordination to Cu(2) must allow for a stronger interaction between S(1) and Ce.

The fact that there are partially occupied Cu tetrahedral sites within the anionic layers suggests the existence of two structurally related compounds: $CuCeS_3$ and $KCeS_3$. The former, with all Cu^+ sites occupied, would have the interlayer galleries cleared of counterions. The latter, provided the extra K^+ could be accommodated between the layers, would have totally empty intralayer grooves. The advantage of both compounds is that they present a great deal of void space, making them prime candidates for intercalation chemistry via reduction of the $(S_2)^{2-}$ to $2S^{2-}$. Li cations would be an appropriate intercalant in either case since their small size gives them access to both the interlayer gallery and the intralayer grooves. Although these phases have yet to be synthesized, we have recently isolated and characterized $NaLnS_3$ (Ln = La, Ce),[17] which has the same $(LnS_3)_n^{n-}$ framework as **I** but is charge balanced by a bilayer of staggered Na^+ ions, leaving the intralayer grooves empty. This suggests that the essential $(LnS_3)_n^{n-}$ framework has a significant stability and that additional lanthanide compounds derived from it may be possible.

Magnetic Susceptibility Studies. The temperature-dependent magnetic susceptibility of **I**, taken at 2000 G over the range 2–300 K, is shown in Figure 4. Curie–Weiss behavior is evident above 160 K with local antiferromagnetic ordering indicated. Extrapolation of the linear portion of the curve (data with $T > 160$ K) yields a Θ of –67 K. Below 160 K, the data deviate negatively from a straight line extrapolated from higher temperatures. This phenomenon has been observed in other Ce^{3+} chalcogenides and has been attributed to crystal field splitting of the cation's $^2F_{5/2}$ ground state.[18] The data conform to a straight line at temperatures above 160 K, and in that region, a μ_{eff} of 3.1 μ_B for **I** was calculated. Since **I** contains formally two Ce^{3+} ions (hence two $4f^1$ electrons) per formula, the μ_{eff} is based on the summation of the susceptibilities of these two ions. By dividing the calculated μ_{eff} by $2^{1/2}$ (since μ_{eff} varies as the square root of χ_M), we estimate a μ_{eff} of 2.2 μ_B per Ce^{3+}. This is close to both the values seen experimentally (2.3–2.5 μ_B) and the calculated theoretical value (2.54 μ_B) for a Ce^{3+} ion.[19] Lanthanides in general have μ_{eff} values which seldom vary with the chemical environment due to the shielding effect the valence orbitals have on the more deeply buried 4f electrons.

(17) Sutorik, A. C.; Kanatzidis, M. G. Work in progress.
(18) Greenwood, N. N.; Earnshaw, A. *Chemistry of the Elements*; Pergamon Press: New York, 1984; p 1443.
(19) (a) Lueken, H.; Bruggemann, W.; Bronger, W.; Fleischhauer, J. *J. Less-Common Met.* **1979**, *65*, 79–88. (b) Duczmal, M.; Pawlak, L. *J. Magn. Magn. Mater.* **1988**, *76–77*, 195–196.

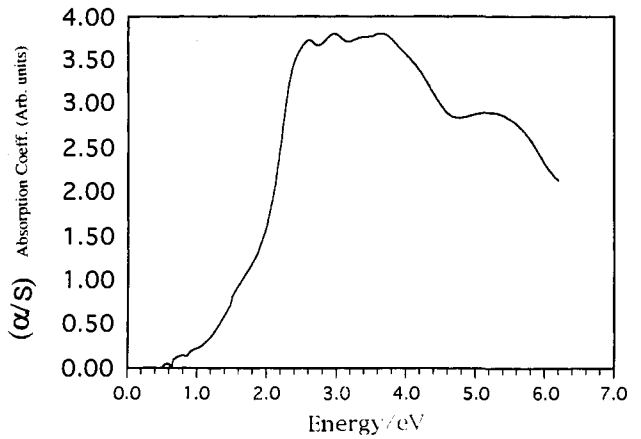

Figure 5. Plot of absorbance (arbitrary units) vs energy (eV) for $KCuCe_2S_6$. The onset of a sharp change in absorbance at 1.8 eV corresponds to an estimate of the material's band gap.

Table 3. Selected Bond Distances (Å) and Angles (deg) for $K_2Cu_2CeS_4$[a]

Ce–S(1)[a]	2.744(1) (×2)	Cu–S(2)[a]	2.418(2)
Ce–S(1)[b,c]	2.737(1)	Cu–S(2)[b]	2.387(1)
Ce–S(2)[c,d]	2.718(2)	Cu–S(2)[c]	2.391(1)
		Cu–S(1)[a]	2.334(2)
S(1)[a]–Ce–S(1)[b]	92.54(6)	S(1)[a]–Cu–S(2)[a]	109.30(7)
S(1)[a]–Ce–S(1)[c]	87.46(6)	S(1)[a]–Cu–S(2)[b]	108.77(5)
S(1)[a]–Ce–S(2)[c]	89.26(4)	S(1)[a]–Cu–S(2)[c]	108.61(5)
S(1)[a]–Ce–S(2)[d]	90.74(4)	S(2)[a]–Cu–S(2)[b]	108.92(5)
S(1)[b]–Ce–S(2)[c]	89.42(4)	S(2)[a]–Cu–S(2)[c]	109.22(5)
S(1)[b]–Ce–S(2)[d]	90.58(4)	S(2)[b]–Cu–S(2)[c]	112.00(8)
Ce–S(1)[b]–Ce[a]	92.54(6)	Cu–S(2)[c]–Cu[b]	112.00(8)
		Cu–S(2)[c]–Cu[a]	71.08(5)
		Cu[a]–S(2)[a]–Cu[b]	70.78(5)

[a] Superscripts indicate symmetry equivalent atoms.

Spectroscopic Data. The optical absorption spectrum of **I** is shown in Figure 5. The onset of a sharp change in α/S at approximately 1.8 eV corresponds to an estimate of the sample's band gap. Hence, **I** is expected to be a semiconductor. This, in conjunction with the magnetic studies, confirms the valence-precise nature of the material, and so its oxidation states can be formalized as $K(Cu^{1+})(Ce^{3+})_2(S^{2-})_2(S_2^{2-})_2$. The tail of absorbance occurring below the band edge may indicate either impurities or the presence of an indirect band gap character which the compound may possess.

The solid-state far-IR spectrum of **I** shows peaks in three regions. A medium strength peak occurs at 473 cm^{-1}, which corresponds to a S–S stretching vibration. Two peaks at 358 and 307 cm^{-1} are very weak and are presumably due to Cu–S bonds, the disordered nature of which probably contributes to their small intensities. Finally, a series of very strong peaks present in the region from 270 to 150 cm^{-1} have been assigned as Ce–S vibrations (namely, 264, 258, 214, 204, and 156 cm^{-1}).

$K_2Cu_2CeS_4$ (II). Structure. The structure of **II** is also layered, with Ce, Cu, and S again forming the anionic layers and K in the interlayer gallery. The Ce ions are octahedrally coordinated in **II**, forming edge-sharing chains in one dimension. These chains are connected into layers via CuS_4 tetrahedra. The $[CuS_4]$ share two edges with octahedra in one chain while forming a corner-sharing connection to an axial S atom on the neighboring chain. The Cu-centered tetrahedra also edge-share with each other, forming a ribbon of anti-PbO structure type between the chains of $[CeS_6]$ octahedra. A view of the extended anionic layers is shown in Figure 6 (a view including K^+ ions is provided in Figure 7), and selected bond distances and angles are given in Table 3.

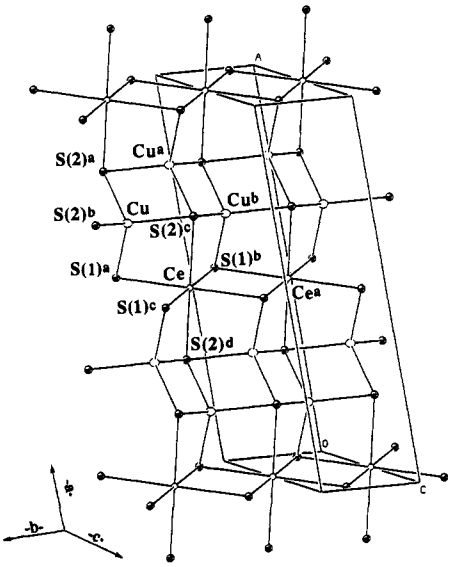

Figure 6. View of a single anionic layer in $K_2Cu_2CeS_4$: small open circles, Ce; large open circles, Cu; circles with octant shading, S. Selected bond distances and angles are given in Table 3.

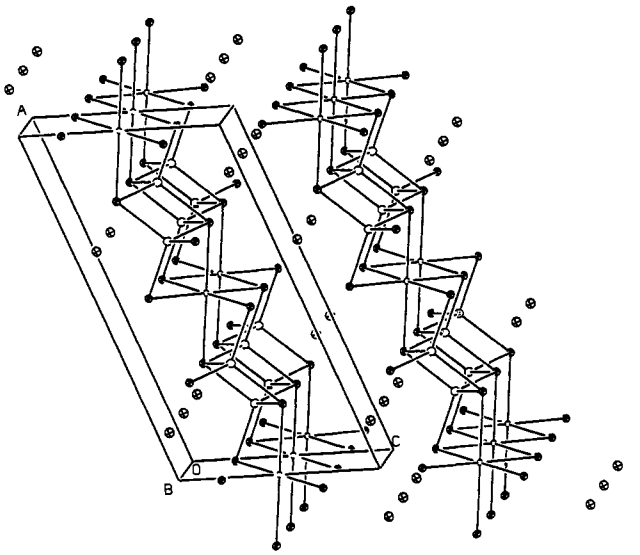

Figure 7. View of the extended structure of $K_2Cu_2CeS_4$, as seen down the *b*-axis: small open circles, Ce; large open circles, Cu; shaded octant circles, S; nonshaded octant circles, K.

Short Cu–Cu contacts are also present (2.785(1) and 2.793(1) Å) and are characteristic of well-known d^{10}–d^{10} interactions.[20]

Although relatively rare for the early lanthanides in general, octahedral coordinations are seen in the $ALnQ_2$ series of compounds which possess either NaCl or α-$NaFeO_2$ structure types.[21] The Ce–S distances for **II** are 2.737(1) and 2.744(1) Å in the equatorial positions and 2.718(2) Å in the axial positions.

(20) (a) Mertz, K. M., Jr.; Hoffmann, R. *Inorg. Chem.* **1988**, *27*, 2120–2127. (b) Jansen, M. *Angew. Chem.* **1987**, *99*, 1136; *Angew. Chem., Int. Ed. Engl.* **1987**, *26*, 1098–1111.

(21) Compounds of the type $ALnQ_2$ (A = Na; Ln = La, Ce, Pr, Nd; Q = S) were first synthesized by Ballestracci and Bertaut[21a] with the range of compounds expanded to include A = Li, K, Rb, Cs, and Tl and Q = Se and several other Ln metals by themselves and others.[21b-h] In general, the compounds with large values for the radius ratio, $R_{Ln^{3+}}/R_{A^+}$, favor the disordered NaCl structure whereas smaller values (0.6–1.2) tend toward the α-$NaFeO_2$ structure type.[19i,j] (a) Ballestracci, R.; Bertaut, E. F. *Bull. Soc. Fr. Mineral. Cristallogr.* **1964**, *87*, 512–516. (b) Ballestracci, R.; Bertaut, E. F. *Bull. Soc. Fr. Mineral. Cristallogr.* **1965**, *88*, 136–141. (c) Ballestracci, R. *Bull. Soc. Fr. Mineral. Cristallogr.* **1965**, *88*, 207–210. (d) Tromme, M. *C. R. Acad. Sci., Ser. C* **1971**, *273*, 849–853. (e) Bronger, W.; Elter, R.; Mans, E.; Schmidt, T. *Rev. Chim. Miner.* **1974**, *10*, 147–152. (f) Kabre, S.; Julien-Pouzol, M.; Guittard, M. *Bull. Soc. Chim. Fr.* **1974**, *10*, 1881–1884. (g) Plug, C. M.; Verschoor, G. C. *Acta Crystallogr.* **1976**, *B32*, 1856–1858. (h) Ohtani, T.; Honjo, H.;

These are unusually short Ce–S bonds for six-coordinate Ce. Poix has tabulated the average Ce–S bond for six-coordinate Ce^{3+} as 2.93 Å,[22] and in $KCeS_2$, which adopts the α-$NaFeO_2$ structure type (a derivative of NaCl), the Ce–S distance is 2.878 Å.[21g] The Cu–S distances in **II** are normal (range, 2.334(2)–2.418(2) Å; average, 2.382(3) Å).

The structure of **II** represents a new structure type but is closely related to that of Mg_2SiO_4 (olivine).[23] Olivine features a hexagonal closest packed net of oxygen with Mg^{2+} occupying one-half the octahedral sites in each layer and Si^{4+} occupying one-fourth of the tetrahedral sites in every other layer. Few ternary chalcogenides adopt this structure,[24] but it has recently been found to form for the quaternary chalcogenides $CaYbInQ_4$ (Q = S, Se),[25] where the Ca^{2+} and Yb^{3+} occupy the Mg^{2+} sites and In^{3+} occupies the Si^{4+} sites. This leads to $(YbInS_4)^{2-}$ layers in a manner similar to those of **II**. The differences between **II** and olivine occur in two ways. First, and most obviously, there are twice as many Td sites occupied in **II** as there are in olivine. Second, while the Td sites in **II** are coordinated to one axial S atom of a neighboring chain of octahedra, in olivine, the analogous bond is made to an equatorial atom. The chains are, thus, shifted away from the olivine type of orientation. This also leads to a different coordination environment around the interlayer K^+, that of a seven-coordinate, irregular polyhedron.

Another closely related structure is $FeTaTe_3$.[26] It possesses layers similar to those in **II** except that $[TaTe_6]$ octahedra form edge-sharing double chains, rather than single chains, which then are linked by edge-sharing $[FeTe_4]$ tetrahedra in the manner of **II**. Such layers were also recently reported for $NaCuTiS_3$ and $NaCuZrQ_3$ (Q = Se, Te).[27]

Although the formal valence charges in **I** balance nicely, uncertainties exist for **II**. Formally, two extremes on the oxidation state of Cu and Ce could exist: either $K_2(Cu^{1+})_2(Ce^{4+})S_4$ or $K_2(Cu^{1+})(Cu^{2+})(Ce^{3+})S_4$. Chemically, neither extreme is favorable since both Cu^{2+} and Ce^{4+} are too oxidizing to exist in conjunction with S^{2-}, and no examples of either have ever been confirmed. Rather than form these high oxidation states, phases tend to either form oxidized disulfide bonds to the extent necessary to achieve charge balance, as in CuS[28] and CeS_2,[29] or possess a mixture of S^{2-} and S^{1-} oxidation states, as in KCu_4S_3.[30] The closest S–S distance in **II** is only 3.783(4) Å, ruling out the possibility of disulfide formation, and so a reasonable formalism may be $K_2(Cu^{1+})_2(Ce^{3+})(S^{2-})_3(S^{1-})$. Such a compound would be paramagnetic, due to the $4f^1$ electron of Ce^{3+}, and if the S^{1-} hole were to be delocalized throughout the sulfur 3p band as in KCu_4S_3, p-type metallic behavior should be observed.[31] The formalism using all Ce^{4+} would be a diamagnetic semiconductor. Hence, magnetic and conductivity measurements would be useful in elucidating the various oxidation state ambiguities present in this compound.

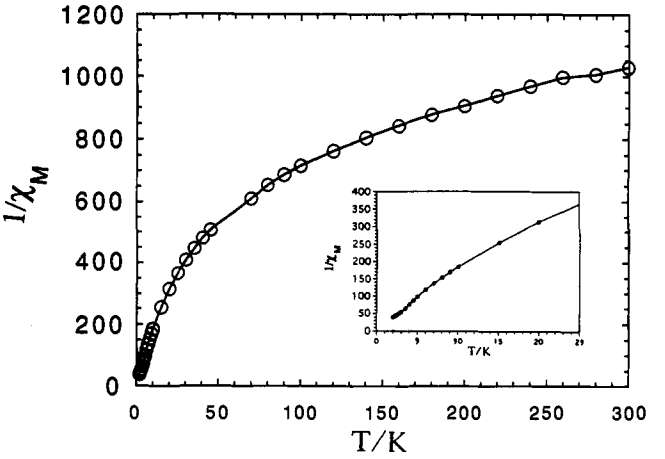

Figure 8. Plot of $1/\chi_M$ vs T for $K_2Cu_2CeS_4$ taken at 1000 G over 2–300 K. The inset graph shows an expanded view of the region 2–25 K.

Spectroscopy. Diffuse optical reflectance measurements on **II** show no absorption edge, and hence no band gap, in the region 250–2500 nm. The level of reflectance remained low (≤10%) throughout the region with both $BaSO_4$ and CdS used as 100% reflectance standards. The solid-state far-IR spectrum of **II** shows three strong peaks, all of which occur in the region of Ce–S stretching: 272, 213, and 159 cm^{-1}. Apparently any IR activity from Cu–S is either too weak to be seen or is simply IR inactive.

Magnetic Susceptibility Studies. The temperature-dependent magnetic susceptibility of **II**, taken at 1000 G over 2–300 K, is shown in Figure 8. No clear Curie–Weiss portion of the data exists although the data drop off much more rapidly below 150 K than above. To estimate the level of magnetization of **II** in the region above 150 K, Curie–Weiss behavior was approximated by applying a linear curve fit to the data, resulting in a μ_{eff} of 2.38 μ_B/formula and a very large Θ of –440 K. This corresponds to the value previously discussed for a Ce^{3+} ion and is consistent with the formalism in which a localized Ce^{3+} is charge balanced by a delocalized S^{1-} state.

As noted in the magnetics of **I**, Ce^{3+} compounds typically have a certain degree of non-Curie–Weiss behavior to their paramagnetic response. The main source of this effect is the weak crystal field splitting of the ion's $^2F_{5/2}$ ground state although it has been shown that different amounts of superexchange are possible through the excited and ground states and that this exchange anisotropy contributes to the shape of the $1/\chi_m$ vs T curve. Such behavior was modeled for the Ce^{3+} in $NaCeS_2$ by Lueken et al.[19] Attempts to fit our data to that model have yet to produce a consistent set of parameters, probably due to small amount of CeO_2 and possibly other impurities present in the microcrystalline samples of **II**. However, such treatments do indicate a large amount of antiferromagnetic superexchange taking place through the excited state, accounting for the large Θ value estimated above. This antiferromagnetic superexchange also accounts for the shape of the $1/\chi_m$ vs T plot. As the excited state is depopulated at low temperature, the effect of antiferromagnetic superexchange through the excited state is decreased. With less antiferromagnetic coupling, the bulk magnetization of the samples rises as the ground state becomes more populated at low temperatures. If this model is accurate, a hole in the sulfur 3p band may play a role in facilitating this exchange as is thought to occur in the spinel compounds $CuCr_2Q_4$ (Q = S, Se, Te).[32]

Charge-Transport Measurements. The mixed S^{2-}/S^{1-} oxidation state model for **II** suggests that the compound would exhibit metallic properties. First we note that the compound is more than 5 orders of magnitude more conductive than $KCuCe_2S_6$,

Wada, H. *Mater. Res. Bull.* **1987**, *22*, 829–840. (i) Bronger, W. *Crystallography and Crystal Chemistry of Materials with Layered Structures*; Levy, F., Ed.; D. Reidel Publishing Co.: Dordrecht, Holland, 1976; p 93. (j) Brunel, M.; DeBergevin, F.; Gondrand, M. *J. Phys. Chem. Solids* **1972**, *33*, 1927–1941.

(22) Poix, P. *C. R. Acad. Sci., Ser. C* **1970**, *270*, 1852–1853.

(23) *Rock-Forming Minerals, Orthosilicates*; Deer, W. A., Howie, R. A., Zussman, J., Eds.; Longman: London and New York, 1982; Vol. 1A.

(24) *Pearson's Handbook of Crystallographic Data for Intermetallic Phases*, 2nd ed.; Villars, P., Calvert, L. P., Eds.; ASM International: Metals Park, OH, 1991; p 232.

(25) Carpenter, J. D.; Hwu, S. J. *Chem. Mater.* **1992**, *4*, 1368–1372.

(26) Liu, S.-X.; Cai, G.-L.; Huang, J.-L. *Acta Crystallogr.* **1993**, *C49*, 4–7.

(27) Mansuetto, M. F.; Keane, P. M.; Ibers, J. A. *J. Solid State Chem.* **1993**, *105*, 580–587.

(28) Berry, L. G. *Am. Mineral.* **1954**, *39*, 504–509.

(29) (a) Ring, S. A.; Tecotzky, M. *Inorg. Chem.* **1964**, *3*, 182–185. (b) Marcon, J. P.; Pascard, R. *C. R. Acad. Sci., Ser. C* **1968**, *266*, 270–272.

(30) Folmer, J. C. W.; Jellinek, F. *J. Less-Common Met.* **1980**, *76*, 153–162.

(31) Brown, D. B.; Zubieta, J. A.; Vella, P. A.; Wrobleski, J. T.; Watt, T.; Hatfield, W. E.; Day, P. *Inorg. Chem.* **1980**, *19*, 1945–1950.

(32) (a) Lotgering, F. K.; van Stapele, R. P. *J. Appl. Phys.* **1968**, *39*, 417–423. (b) Hollander, J. C. Th.; Sawatzky, G.; Haas, C. *Solid State Commun.* **1974**, *15*, 747.

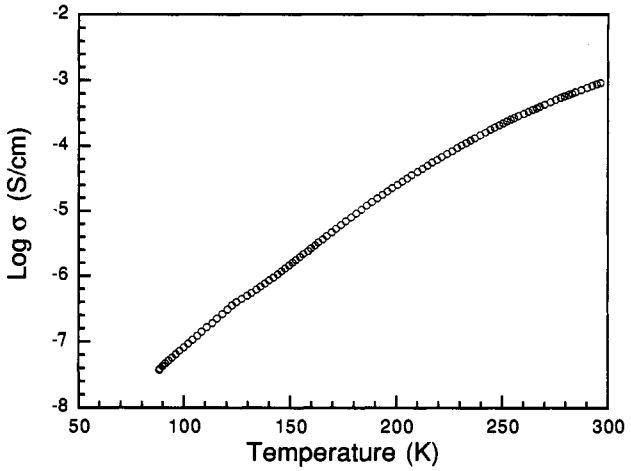

Figure 9. Variable-temperature four-probe conductivity data for a pressed pellet of $K_2Cu_2CeS_4$.

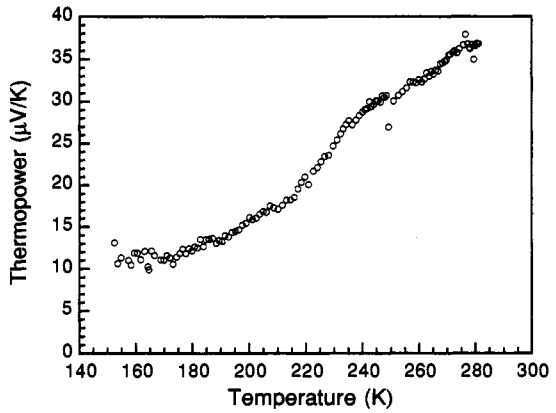

Figure 10. Variable-temperature thermopower data for $K_2Cu_2CeS_4$ taken on a pressed pellet of microcrystalline sample.

which is nearly an insulator. The metallic behavior, however, is not supported by conductivity measurements either on single crystals or on pressed pellets. Interestingly, the results from a single crystal were similar to those of the pellet probably because the small crystal size does not allow for reliable electrode contact to be made. Variable-temperature measurements, shown in Figure 9, reveal decreasing conductivity with falling temperatures, the characteristic behavior of semiconductors rather than metals. The low magnitude of the room temperature conductivity (ca. 10^{-3} S/cm) also indicates semiconducting behavior. These results were consistently reproduced using material from different synthetic batches.

Although the effects of grain boundaries in the polycrystalline pellets generally complicate the interpretation of electrical conductivity data, this is not the case with thermoelectric power (TP) measurements.[33] A complimentary probe used to investigate the charge-transport properties of **II** was the TP response as a function of temperature. TP measurements are very reliable in determining a sample's charge-transport type because the technique is essentially zero-current and as such independent of sample defects or grain boundaries.[33] The TP response of a polycrystalline pressed pellet of **II** is shown in Figure 10. The positive values confirm that holes are the dominant charge carriers, and this is in keeping with the mixed-valent model which places holes on the sulfur p-band. Although the trend of a decreasing TP tending toward zero with falling temperature is consistent with metallic behavior, the magnitude of the TP values is much larger than would be expected for a metallic compound. Below 150 K, the sample became too resistive to give reliable data.

Explanations for these results lie in considering the pathways of conduction through the structure of **II**. Although discussed as a layered material, conduction would in fact primarily take place via the chains of edge-sharing $[CuS_4]$ tetrahedra. This is because the Ce^{3+} are largely ionic in their bonding, with the 4f orbitals buried among the core electrons and the valence 5d, 6s, and 6p orbitals too high in energy to contribute significantly to the valence band comprised mainly of sulfur 3p orbitals. Therefore, the valence band along directions parallel to the layers would be extremely narrow. A two-dimensional conduction pathway for **II** would make it very susceptible to crystal defects which could rupture the conduction pathways. Conduction would then rely on thermal excitation of electrons across defect boundaries, leading to a semiconductor style response.

Although undoubtedly a factor, defects and misoriented crystals do not account for the high values of the TP measurements because the technique is less dependent on such variables. A further explanation is that the very narrow valence bands of **II** may be enough to result in the formation of small polarons in the material. A polaron is simply a charge carrier, be it electron or hole, which is trapped in the potential which it induces in the field around it. The mobility of the carrier is then limited by having to drag the induced field around with it, leading to hopping conduction.[34] Key to the formation and subsequent low mobility of small polarons is a very narrow band for the polaron to travel in and the presence of highly charged cations or anions, in this case Ce^{3+}. This increases the effective mass of the carrier and decreases the mean free path of the polaron. Hence, formation of small polaron-like species leads to the effective localization of the carrier and conduction can only proceed via thermal excitation from site to site. Such behavior has been described theoretically by Austin and Mott[35] and studied in semiconducting $Na_xV_2O_5$[36] bronzes and $V_2O_5{\cdot}nH_2O$ xerogels.[37] Usually the phenomenon is used to explain semiconducting properties in transition metal oxides which, through crystal defects, possess a small amount of metal ions in mixed oxidation states. Such a conducting mechanism would explain the observed behavior in **II**. If localized as small polarons, then some unusual coupling scheme must be rendering S^{1-} magnetically silent as well. This could also contribute to the sharply deviating $1/\chi_m$ vs T response already discussed. The small polaron-like character of the holes may be decreased or suppressed if the S--S distance about the Ce^{3+} centers can be decreased, which may be possible by changing the size of the other elements in the structure such as the alkali cation or the Cu. This in turn could lead to higher and possibly metal-like conductivities.

In the cases of $KCuCe_2S_6$ and $K_2Cu_2CeS_4$, the combination of the electropositive alkali metal and lanthanide did not cause an increase in the oxidation state of the copper as seen in high-T_c superconducting oxides. The reason simply lies in the decrease in electronegativity upon going from oxygen to sulfur. However, as seen in this and previous work, the Cu–S bond is fundamentally different in that Cu^{2+} is not stable in an environment of solely S^{2-} ions. Hence, the covalency of such bonds is limited to what can be achieved with Cu^+, and increases in covalency analogous to those in the high-T_c oxides may not be achievable, even with added induction from highly electropositive cations. Perhaps, in the class of chalcogenides, transition metals other than copper may be more suitable for emulating the effects operating in the copper oxides.

(33) (a) Marks, T. J. *Angew. Chem., Int. Ed. Engl.* **1990**, *29*, 857–879. (b) Almeida, M.; Gaudiello, J. G.; Kellog, G. E.; Tetrick, S. M.; Marcy, H. O.; McCarthy, W. J.; Butler, J. C.; Kannewurf, C. R.; Marks, T. J. *J. Am. Chem. Soc.* **1989**, *111*, 5271–5284.

(34) Dougier, P.; Fan, J. C. C.; Goodenough, J. B. *J. Solid State Chem.* **1975**, *14*, 247–259.

(35) (a) Austin, I. G.; Mott, N. F. *Adv. Phys.* **1969**, *18*, 41–99. (b) Mott, N. F. *J. Non-Cryst. Solids* **1968**, *1*, 1–17.

(36) Badot, J. C.; Gourier, D.; Bourdeau, F.; Baffier, N.; Tabuteau, A. *J. Solid State Chem.* **1991**, *92*, 8–17.

(37) Livage, J. *Chem. Mater.* **1991**, *3*, 578–593.

Concluding Remarks

The isolation of $KCuCe_2S_6$ and $K_2Cu_2CeS_4$ suggests several intriguing possibilities for future synthetic work. Lanthanides in general are chemically very similar, and so the formation of a series of compounds with the formulas $KCuLn_2S_6$ and $K_2Cu_2LnS_4$ (Ln = lanthanide) is feasible.[38] Also intriguing is the possible ionic conductivity which the Cu^+ disorder in $KCuCe_2S_6$ presents. Aside from being an interesting physical property, such conductivity could allow for other materials to be formed via ion exchange, either alone or in conjunction with a partial reduction of the compound's $(S_2)^{2-}$ ligands, possibly leading to metallic properties in the altered compounds. These manipulations could easily be performed under mild synthetic conditions and so could lead to a series of metastable compounds which may be inaccessible even by using molten polychalcogenide techniques. Although Cu in $K_2Cu_2CeS_4$ did not experience unusually high oxidation states, II implies that another criterion for superconductivity may in fact be accessible: the formation of narrow bands with high density of states at the Fermi level. Although narrow valence bands in II seem to be limiting the mobility of the S^{1-} holes, it may be possible to synthetically adjust the composition of the phase so that a metal-like character is introduced. This causes us to speculate on the possibility of related phases here. Conceptually, compounds of the type $A_x[Cu_2S_2]_n[CeS_2]_m$ could be synthesized which contain either wider fragments of $[CeS_6]$ octahedra (narrowing the valence band) or wider fragments containing $[CuS_4]$ tetrahedra (resulting in greater orbital overlap and wider bands). The successful synthesis of $KCuCe_2S_6$ and $K_2Cu_2CeS_4$ opens the door to the exploration of these and other possibilities.

Acknowledgment. The authors wish to gratefully acknowledge the National Science Foundation (DMR-9202428), the Ford Foundation, and the NASA Graduate Fellowship Research Program for financial support. The work at Northwestern made use of the MRL Central Facilities supported by the NSF at the Materials Research Center under Award No. DMR-91-20521. We also wish to thank Dr. Hwu for the sharing of preprinted material.

Supplementary Material Available: Tables of calculated and observed X-ray powder diffraction patterns, fractional atomic coordinates, and anisotropic thermal parameters (7 pages); listings of calculated and observed structure factors (12 pages). This material is contained in many libraries on microfiche, immediately follows this article in the microfilm version of the journal, and can be ordered from the ACS; see any current masthead page for ordering information.

(38) $KCuLa_2S_6$ has been recently prepared and found to be isostructural with I via X-ray powder diffraction, although the amount of Cu^+ disorder cannot be known without single crystal analysis. The structures of $CsCuCe_2S_6$ and $KCuCe_2Se_6$ have been determined with single crystal X-ray diffraction. They possess the same structure as I but crystallize in the more symmetric orthorhombic space group *Immm* (no. 71). ($CsCuCe_2S_6$: a = 5.500(1) Å, b = 22.45(1) Å, c = 4.205(4) Å, V = 519.3(6) Å^3, R/R_w = 3.4/4.3%. $KCuCe_2Se_6$: a = 5.695(1) Å, b = 22.236(6) Å, c = 4.297(2) Å, V = 544.1(3) Å^3, R/R_w = 3.5/4.2%.) In these phases the Cu^+ is again disordered, refining at 50% occupancy at all sites in the intralayer grooves. Compounds isostructural to $K_2Cu_2CeS_4$ have yet to be observed: Sutorik, A. C.; Kanatzidis, M. G. Work in progress.